IISE Transactions on Occupational Ergonomics and Human Factors

ISSN: (Print) (Online) Journal homepage: https://www.tandfonline.com/loi/uehf21

Model-Based Comparison of Passive and Active Assistance Designs in an Occupational Upper Limb Exoskeleton for Overhead Lifting

Xianlian Zhou & Liying Zheng

To cite this article: Xianlian Zhou & Liying Zheng (2021) Model-Based Comparison of Passive and Active Assistance Designs in an Occupational Upper Limb Exoskeleton for Overhead Lifting, IISE Transactions on Occupational Ergonomics and Human Factors, 9:3-4, 167-185, DOI: 10.1080/24725838.2021.1954565

To link to this article: https://doi.org/10.1080/24725838.2021.1954565

IISE TRANSACTIONS ON OCCUPATIONAL ERGONOMICS AND HUMAN FACTORS
2021, VOL. 9, NOS. 3–4, 167–185
https://doi.org/10.1080/24725838.2021.1954565

Taylor & Francis
Taylor & Francis Group

METHODS, MODELS, & THEORIES

Model-Based Comparison of Passive and Active Assistance Designs in an Occupational Upper Limb Exoskeleton for Overhead Lifting

Xianlian Zhou[a] and Liying Zheng[b]

[a]Department of Biomedical Engineering, New Jersey Institute of Technology, Newark, NJ, USA; [b]Health Effects Laboratory Division, National Institute for Occupational Safety and Health, Morgantown, WV, USA

OCCUPATIONAL APPLICATIONS

In recent years, various upper limb exoskeletons have been developed aiming to support industrial workers for a range of tasks and reduce risks of work-related musculoskeletal disorders. Most commercially available upper limb exoskeletons are passive systems that use compliant elements such as springs or elastic components to store and release energy to assist the user's motion. In contrast, many active exoskeletons, which are typically comprised of one or more powered actuators to provide joint assistance, are still in the research and development stages. Nevertheless, the functions and efficacy of various exoskeleton systems need to be further compared and assessed. This study presents a model-based approach to evaluate different designs of passive and active assistance and demonstrates the benefits of both assistance methods in an overhead lifting task. In addition, the modeling and simulation indicate the potential advantages of using the active assistance, based on electromyography.

TECHNICAL ABSTRACT

Background: In the literature, efficacy of passive upper limb exoskeletons has been demonstrated in reduced activity of involved muscles during overhead occupational tasks. However, there are fewer studies that have investigated the efficacy of active upper limb exoskeletons or compared them with their passive counterparts.

Purpose: We aimed to use an approach simulating human-exoskeleton interactions to compare several passive and active assistance methods in an upper limb exoskeleton and to evaluate how different assistance types affect musculoskeletal loadings during overhead lifting.

Methods: An upper-extremity musculoskeletal model was integrated with a five degree-of-freedom exoskeleton for virtual human-in-the-loop evaluation of exoskeleton design and control. Different assistance methods were evaluated, including spring-based activation zones and active control based on EMG, to examine their biomechanical effects on musculoskeletal loadings including interaction forces and moments, muscle activations, and joint moments and reaction forces.

Results: Our modeling and simulation results suggest the effectiveness of the proposed passive and active assistance methods in reducing biomechanical loadings—the upper-limb exoskeletons could reduce maximum loading on the shoulder joint by up to 46% compared to the no-exoskeleton situation. Active assistance was found to outperform the passive assistance approach. Specifically, EMG-based active assistance could assist over the whole lifting range and had a larger capability to reduce deltoid muscle activation and shoulder joint reaction force.

Conclusions: We used a modeling and simulation approach to virtually evaluate various exoskeleton assistance methods without testing multiple physical prototypes and to investigate the effects of these methods on musculoskeletal loadings that cannot be measured directly or noninvasively. Our findings offer new approaches for testing methods and improving exoskeleton designs with "smart" controls. More research is planned to further optimize the exoskeleton control strategies and validate the simulated results in a real-life implementation.

ARTICLE HISTORY
Received 9 March 2021
Accepted 8 July 2021

KEYWORDS
Overhead lifting; upper limb exoskeleton; musculoskeletal model; human-exoskeleton interaction

1. Introduction

Work-related musculoskeletal disorders (MSDs) in the upper extremities, including the shoulders and arms, are common ailments among occupational workers in the United States (Bureau of Labor Statistics, 2018). It is well accepted that overexertion and repetitive motion

CONTACT Xianlian Zhou alexzhou@njit.edu Department of Biomedical Engineering, New Jersey Institute of Technology, Newark, NJ 07102, USA.

are common events or exposures leading to work-related MSDs. Among different activities involving the shoulder, overhead motions such as lifting are especially strenuous and can cause muscle fatigue in a short duration and pain and injuries in the long term (Bernard & Putz-Anderson, 1997; Chopp et al., 2010; Miranda et al., 2005; Punnett et al., 2000). Among patients with shoulder pain, 69% of them did jobs involving large anteversion angles in the shoulder joint (Grieve & Dickerson, 2008). Despite the associated high risks of shoulder MSDs, repetitive overhead tasks are often inevitable in the occupational settings, such as in automobile assembly or block lifting and placement during masonry jobs. Repetitive overhead lifting is harmful or injurious to the shoulder due to both high muscle activation and the consequent increased internal forces. Prolonged, high level muscle activation can cause fatigue and overuse injury, while high internal forces can cause acute or chronic joint pain and injury. Therefore, a key factor in lowering the risk of injury is to reduce muscle demand and internal joint loadings during these activities.

In recent years, exoskeletons or exosuits are becoming a new frontier of interdisciplinary research in augmenting human performance and assisting human motions to reduce fatigue or prevent injuries (Del Ferraro et al., 2020; McFarland & Fischer, 2019; Zhu et al., 2021). Newly-developed industrial exoskeletons can provide assistance for a range of tasks and help reduce the risks of work-related MSDs (Bogue, 2018; de Looze et al., 2016; Nussbaum et al., 2019), and several commercial exoskeletons have been studied in terms of their effectiveness for assisting overhead tasks (Alabdulkarim & Nussbaum, 2019; Kim et al., 2018a, 2018b; Maurice et al., 2020;; Schmalz et al., 2019). The wide use of upper limb exoskeletons in industry and other settings has been reviewed by others (Gopura et al., 2011, 2016; Islam et al., 2017; Lo & Xie, 2012; McFarland & Fischer, 2019). Most exoskeletons can be classified as passive or active systems. Active systems are typically comprised of one or more powered actuators to provide joint assistance, whereas passive systems use compliant elements such as springs or elastic components to store and release energy and provide timely assistance to the user's motion.

In contrast to the passive exoskeleton products on the market, many active upper limb exoskeletons are still in the research and development stages. For active exoskeletons, designing an intelligent scheme for intention recognition and responsive actuation is a very important but challenging task, due to the complexity and variability of human movement and potential safety concerns. Many researchers have chosen methods based on surface electromyography (EMG) for user intention classification and/or actuation control, as it directly reflects muscle activity levels in real time. Most EMG-based control methods are continuous real-time control, often referred to as proportional myoelectric control (Fougner et al., 2012). Kiguchi and Hayashi (2012) developed an EMG-based, impedance control for an upper-limb power-assist exoskeleton robot, in which EMGs from 16 muscles were used to estimate joint torques. Rahman et al. (2015) developed EMG-based control of a robotic exoskeleton for assisting shoulder and elbow motions, wherein the EMG signals were scaled linearly to estimate virtual joint torques and subsequently desired joint positions. Tang et al. (2014) developed a pneumatic, muscle actuated upper-limb power-assist exoskeleton, using proportional myoelectric control based on real-time measurements of EMG from four muscles and a neural network that predicted the target elbow angle based on EMG features. Li et al. (2014) presented two EMG-based force control strategies for an upper-limb power-assist exoskeleton—one was based on the agonist and antagonist muscle forces and the other involved a motion-type classifier. Later, Li et al. (2017) developed an adaptive impedance control method for an upper limb robotic exoskeleton, using a musculoskeletal model driven by surface EMG.

Simulation-based studies have been utilized to examine the design and evaluate the effectiveness of various exoskeletons, using human modeling software such as OpenSim (Delp et al., 2007; Dembia et al., 2017), AnyBody (Damsgaard et al., 2006; Zhou et al., 2015), and JackEx (Constantinescu et al., 2016, 2019). In this study, we adopted a human-exoskeleton interaction simulation approach to compare a series of passive and active assistance designs in an upper limb exoskeleton and to evaluate how different assistances affect the user's musculoskeletal (MSK) loadings during overhead lifting. By using the modeling and simulation approach, we could virtually evaluate different exoskeleton control designs without making multiple physical prototypes, which could significantly reduce manufacturing cost and time. Firs, we integrated an upper-extremity MSK model with a shoulder exoskeleton and modeled their interactions with elastic bushing elements. Then, two types of assistance strategies—spring-based passive assistance and EMG-based active assistance—were employed, and a hybrid dynamics simulation method was developed. The effects of these assistances on MSK loadings during an overhead lifting task were evaluated by examining

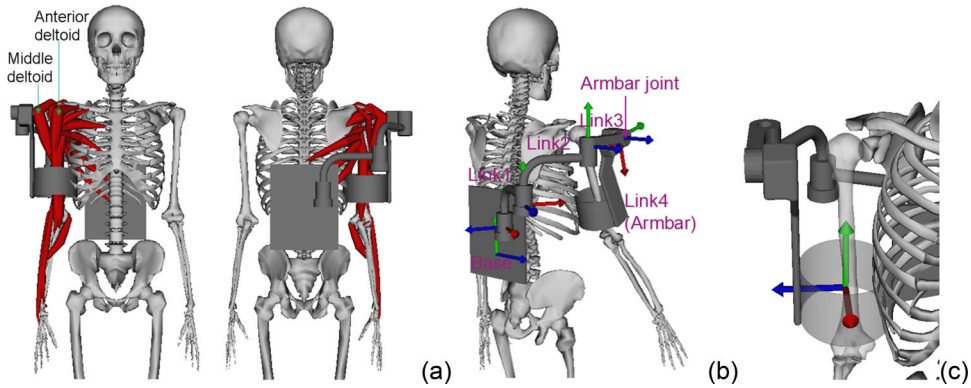

Figure 1. (a) Integration of an upper extremity musculoskeletal model (Saul et al., 2015) with the exoskeleton; (b) The exoskeleton has 5 components with a base connected to the human torso. The local XYZ axes of each link are shown in red, blue, and green, respectively; (c) The bushing frame between the exoskeleton (Link 4) and human upper arm.

predicted muscle activations and shoulder joint muscle torques and reaction forces. By varying the assistance parameters, we also investigated potential optimal control strategy of the present exoskeleton.

2. Methods

2.1. Integrated Exoskeleton and Upper Extremity Musculoskeletal Models

The shoulder exoskeleton model employed here was created using a commercially-available upper-limb exoskeleton as the template, but it was not an exact digital replica (Figure 1). The exoskeleton has five components including one base and four links. The base is attached to the human torso with one translational degrees-of-freedom (DOF) to only allow up and down movement. The exoskeleton has four rotational DOFs, one for each link (1 to 4). The joint axis for links 1 to 3 is along the Y or vertical axis, whereas the joint axis of link 4 (i.e., armbar) is along the Z or lateral axis (Figure 1b). Link 4 is strapped elastically onto the human upper arm. The total mass of the exoskeleton was estimated to be 4.30 kg, and the inertial properties of each component (Table 1) were derived from material and geometry based on the method by Mirtich (1996). The exoskeleton model was assembled onto a MSK model of the upper extremity developed by Saul et al. (2015), which uses the dynamic muscle model described by Schutte et al. (1993).

To simulate overhead lifting, we obtained data for a lifting motion (Mokrani, 2009) from one representative subject with shoulder elevation and elbow angles shown in Figure 2. The subject sequentially retracted the shoulder backwards, flexed the elbow, elevated the shoulder, and then extended the elbow to lift the object overhead. The total lifting time was 1.5 seconds, with ascending elevation in the middle. In the last ~0.3 seconds, both the shoulder elevation and elbow angles were kept steady to place the object. Since only two joint angles were used in the sagittal plane, motions in the other two planes were not considered in the simulation.

Table 1. Mass and inertia (unit: $kg\ m^2$) properties of the exoskeleton.

	Mass (kg)	Ixx ($x10^{-2}$)	Iyy ($x10^{-2}$)	Izz ($x10^{-2}$)
Base	2.200	3.114	1.533	1.629
Link 1	0.498	0.035	0.311	0.339
Link 2	0.391	0.030	0.258	0.284
Link 3	0.213	0.003	0.056	0.056
Link 4	1.000	0.212	2.240	2.199

2.2. Modeling of Human-Exoskeleton Interaction

The human and exoskeleton are often tied together with elastic straps. Previously, we have used a direction-dependent, spring-damper element that connects corresponding anchor points on the body and exoskeleton to generate translational forces between the human and strap (Zhou & Chen, 2021). In this study, we augmented that approach with additional rotational or torsional moments generated by the strap, which effectively makes it a bushing element that generates forces or moments due to the deviation between two frames. Figure 1c shows these two bushing frames that are coincident—one is on the human upper arm and the other is on Link 4 of the exoskeleton. The bushing forces and moments generated were modeled by translational and rotational springs and dampers with linear coefficients:

$$\begin{cases} f_x = k_x x + c_x \dot{x} \\ f_y = k_y y + c_y \dot{y} \\ f_z = k_z z + c_z \dot{z} \end{cases} \quad \text{and} \quad \begin{cases} \tau_x = \alpha_x \theta_x + \beta_x \dot{\theta}_x \\ \tau_y = \alpha_y \theta_y + \beta_y \dot{\theta}_y \\ \tau_z = \alpha_z \theta_z + \beta_z \dot{\theta}_z \end{cases} \quad (1)$$

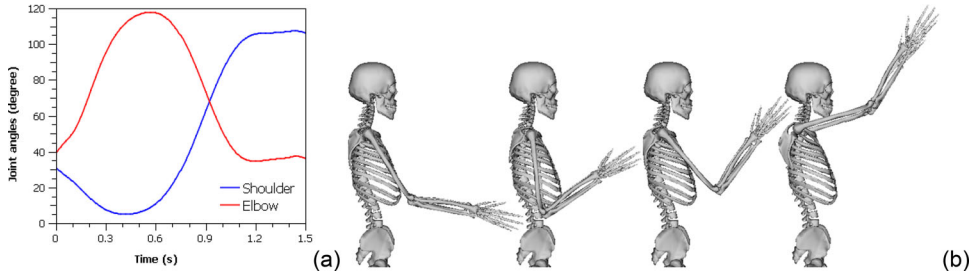

Figure 2. (a) Shoulder elevation and elbow angles during the overhead lifting motion; (b) snapshots of the motion at 0, 0.4, 0.8, and 1.2 seconds. The shoulder (elevation) angle is 0° when the arm points downward and 90° when the upper arm is horizontal.

Table 2. Parameters for the upper arm bushing. Units for translational stiffness and damping are N/m and $N \cdot s/m$, respectively and for rotational stiffness and damping are $Nm/radian$ and $Nm \cdot s/radian$, respectively.

	Translation			Rotation (Nm/radian)		
	X	Y	Z	X	Y	Z
Stiffness	5000	500	5000	100	10	100
Damping	50	5	50	20	2	20

where f_x, f_y, and f_z, are the translational forces; τ_x, τ_y, and τ_z are the rotational/torsional moments along the bushing frames; $x, y, and\ z$ are the translation distances between the origins of the two frames; θ_x, θ_y, and θ_z are the x-y-z body-fixed Euler angles between the frames; and k_i, c_i, α_i, and β_i $(i = x, y, z)$ are directional linear constants. The latter directional constants allowed us to model different resistance strengths of the strap along different directions. Bushing parameters for the upper arm strap are listed in Table 2. For the connection between the base of the exoskeleton and the human torso, we used another bushing element to simulate the effect of shoulder and waist straps. Since the base can only move in the vertical direction without rotation and lateral movement (an assumption made for symmetry), the bushing element was treated as a one-dimensional spring-damper force. The stiffness and damping for this bushing were $5000N/m$ and $100N \cdot s/m$, respectively.

2.3. Exoskeleton Assistances

Two exoskeleton assistance methods were investigated. The first one is a passive, spring-based activation zone illustrated in Figure 3. When the armbar angle (θ) is between θ^L_{min} and θ^H_{min}, the spring generates a lifting torque at the armbar joint. The torque increases linearly from zero at θ^L_{min} to a maximum torque at θ_{max} and then linearly decrease to zero again at θ^H_{min}. We created three different activation zones – Low, Mid (Middle) and High – with parameters listed in Table 3. All three activation zones have the same maximum torque of $20Nm$.

The second assistance method is an EMG-based active approach that generates the armbar joint torque based on the activity of the anterior deltoid muscle, assuming a powered actuator is equipped at the armbar joint. The armbar joint torque is proportional to the activation of the anterior deltoid (act_{AD}), with a linear coefficient p :

$$\tau = \begin{cases} 0, & act_{AD} \leq \epsilon \\ p \times act_{AD}, & act_{AD} > \epsilon \end{cases}, \tag{2}$$

where p is a control parameter that can be tuned, and act_{AD} in practice is estimated from the muscle's processed and normalized EMG signal ($0 \leq act_{AD} \leq 1$). The number ϵ is the activation threshold, which was set as 0.1, or 10% of the maximum voluntary contraction (MVC), and was used to avoid torque assistance due to small EMG signal noise or antagonistic co-activation (Assila et al., 2020; Blache et al., 2015).

2.4. Simulation Methods

A hybrid inverse dynamics (ID) and forward dynamics (FD) simulation framework was employed, similar our previous work (Zhou et al., 2014; Zhou & Chen, 2021). Due to the lack of experimental data, we assumed that the human kinematics did not change even with the assistance of an exoskeleton, and a similar assumption was made in other studies (Dembia et al., 2017; Uchida et al., 2016). The human joints were classified as ID joints, such that their motions were prescribed to track the given input motion, whereas the exoskeleton joints were classified as FD joints, such that their motions were driven by the actuation or interaction forces. The predicted ID joint torques were the desired torques that ideally shall be generated from the muscles spanning these joints. Due to the redundancy of the muscles, muscle forces were determined by solving an optimization problem that minimizes the following objective function:

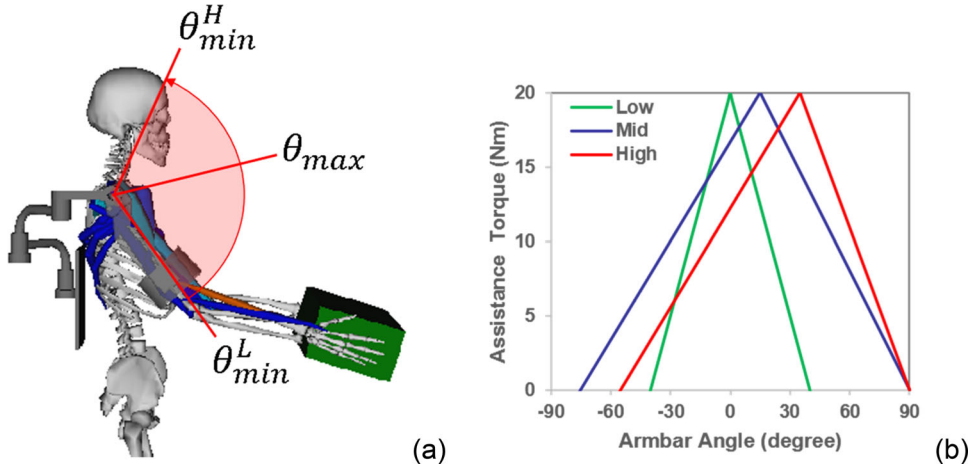

Figure 3. (a) Illustration of the activation zone. (b) Three different activation zones with a maximum torque of $20\boldsymbol{Nm}$. The armbar angle (θ) is zero when the upper arm is horizontal.

Table 3. Parameters for the three activation zones (unit: degree).

	Low	Middle	High
θ^L_{min}	−40	−75	−55
θ_{max}	0	15	35
θ^H_{min}	40	90	90

$$\sum_{i=1}^{n}\left(\frac{f_i}{f_i^{max}}\right)^p + w_U\sum_{j=1}^{m}\sum_{i=1}^{n} f_i||\boldsymbol{U}_i^j|| + w_R||\boldsymbol{R}|| \quad (3)$$

where n is the total number of muscles, f_i is the force of the i-th muscle, f_i^{max} is the maximum attainable muscle force at its current state, $\boldsymbol{R}$ is the residual torque indicating the difference between the desired joint moments and the muscles generated moments, and w_R is a weighting or penalty factor. The second term is an objective associated with the joint reaction forces, in which $\boldsymbol{U}_i^j$ is the joint reaction force induced by a unit force along the path of f_i, and $m = 2$ indicates the two joints (shoulder and elbow) considered. In all simulations, we set $p = 2$ (Erdemir et al., 2007), $w_U = 0.01$, and $w_R = 100$ (Zhou & Chen, 2021). Once the optimized forces (f_i) were found, muscle excitations were estimated based on current muscle states, and consequently muscle activations were computed based on the excitation-activation mechanism. In the EMG-based active control, the predicted anterior deltoid muscle activation (act_{AD}) was used for computing the exoskeleton joint torque according to Eq. (2). An in-house, extended version of the musculoskeletal simulation code CoBi-Dyn, originally developed at CFD Research Corporation (Huntsville, AL)(Zhou et al., 2014; Zhou & Chen, 2021), was used to perform the simulations.

We first conducted a simulation of overhead lifting a 10 kg mass without the exoskeleton to establish the baseline. We then conducted a simulation with the exoskeleton in a fully passive mode without any assistance turned on (i.e., no passive or active assistance), as shown in Figure 4. The box is presented for visualization to represent the 10 kg mass. In the simulation, a 5 kg mass was placed at the carpal location of each hand, assuming even weight distribution. Then, we conduct three spring-assist passive simulations with Low, Middle, and High activation zones (Figure 3), followed by another three simulations of the EMG-based active assistance with the proportional gain p in Eq. (2) equal to 25, 50, and 100. According to our tests, these three values represent three distinctive active control levels: low, middle, and high. In total, there were eight simulations, including no exoskeleton (NoExo), fully passive exoskeleton without assistance (PassiveExo), spring-based passive assistances with three activation zones (Low, Mid, and High), and EMG-based active assistances with three EMG gains (Low, Mid, and High).

3. Results

In all the exoskeleton-involved simulations, the armbar joint angles were relatively close to each other due to the bushing constraint of the strap and the pre-prescribed motion of the human arms (Figure 5). As shown in Figure 6, the bushing forces and moments for the PassiveExo case are much smaller than those cases with assistance. The largest bushing force (moment) between the exoskeleton armbar and human for the passive case was lower than 10 N (3Nm), while the largest bushing force (moment) for the high-EMG-gain active case was greater than 50 N (18Nm).

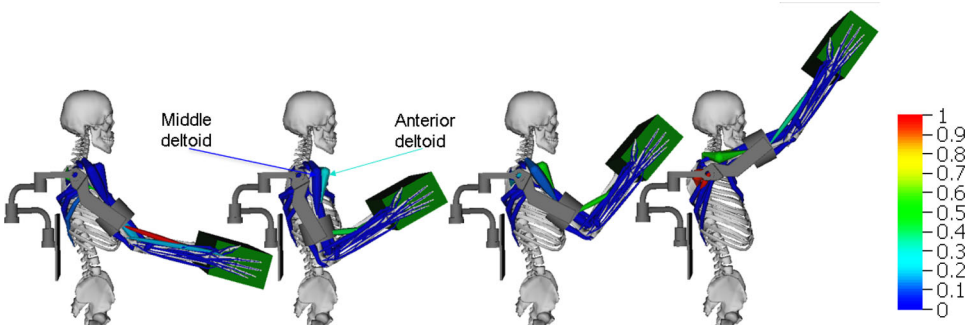

Figure 4. Snapshots of the simulation of an overhead lifting motion with a fully passive exoskeleton (PassiveExo) at 0, 0.4, 0.8, and 1.2 seconds. The color code of muscle activations (0-1) is shown on the right.

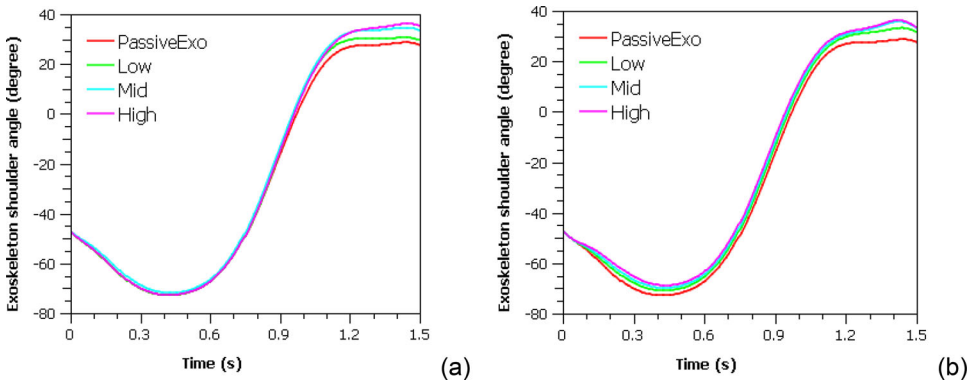

Figure 5. Armbar joint angles for (a) the spring-assist passive cases and (b) the EMG-based active cases. The PassiveExo (fully passive exoskeleton without assistance) case is present in both figures as the reference.

Predicted human shoulder joint moments for all eight simulations are shown in Figure 7(a and b). By subtracting the baseline joint moment of the NoExo case, we obtained the differences for all other cases, as shown Figure 7(c and d). The PassiveExo case increased the shoulder moment slightly during the entire motion, except at the very beginning when the arm started to retract. For the spring-assist cases (Figure 7c), the moments were reduced mostly during the late stage when the armbar joint angle entered the respective activation zones. For the Mid and High cases, small moment reductions were observed at the beginning as well, since the exoskeleton was within the two activation zones before arm retraction. The maximum reductions were all close to but still smaller than $20Nm$. Unlike the other two cases, in which moment reductions diminished as the exoskeleton entered the decline region of their activation zones, the High activation zone case retained a high reduction at the end of the simulation since the armbar angle was close to the θ_{max} (35°). On the other hand, the EMG-assist cases reduced the shoulder joint moment across the board, with a maximum reduction of 24.5Nm (Figure 7d).

Exoskeleton joint torques generated by the spring assistances and the EMG-based assistances are shown in Figure 8(a and b). The largest joint torques generated by the spring assistances are all at $20Nm$, since the armbar angles all passed the θ_{max} of their respective zones. The largest joint torques generated EMG-based assistances of $\sim 25Nm$ for both the Mid and High cases, while the Low case produced $\sim 14Nm$. Compared to the human shoulder joint moment reductions in Figure 7(c and d), the patterns of corresponding assistance torques were very similar (with a sign difference), but the magnitudes were slightly higher.

We investigated the mechanical powers of the assistance torques, which were computed as the product of the armbar joint torque and its angular velocity, and the results are shown in Figure 8(c and d). For the spring-assist passive cases, small negative powers were generated at the beginning and the end of the simulation. For the EMG-based active cases, larger negative powers were generated during a similar time frame. Since all the joint torques were positive, the negative powers were generated due to negative velocities during the initial arm retraction and the last phase of weight placement. To estimate how much of these mechanical powers were transmitted to the human shoulder joint, we computed the (human) assistance powers as the product of the shoulder

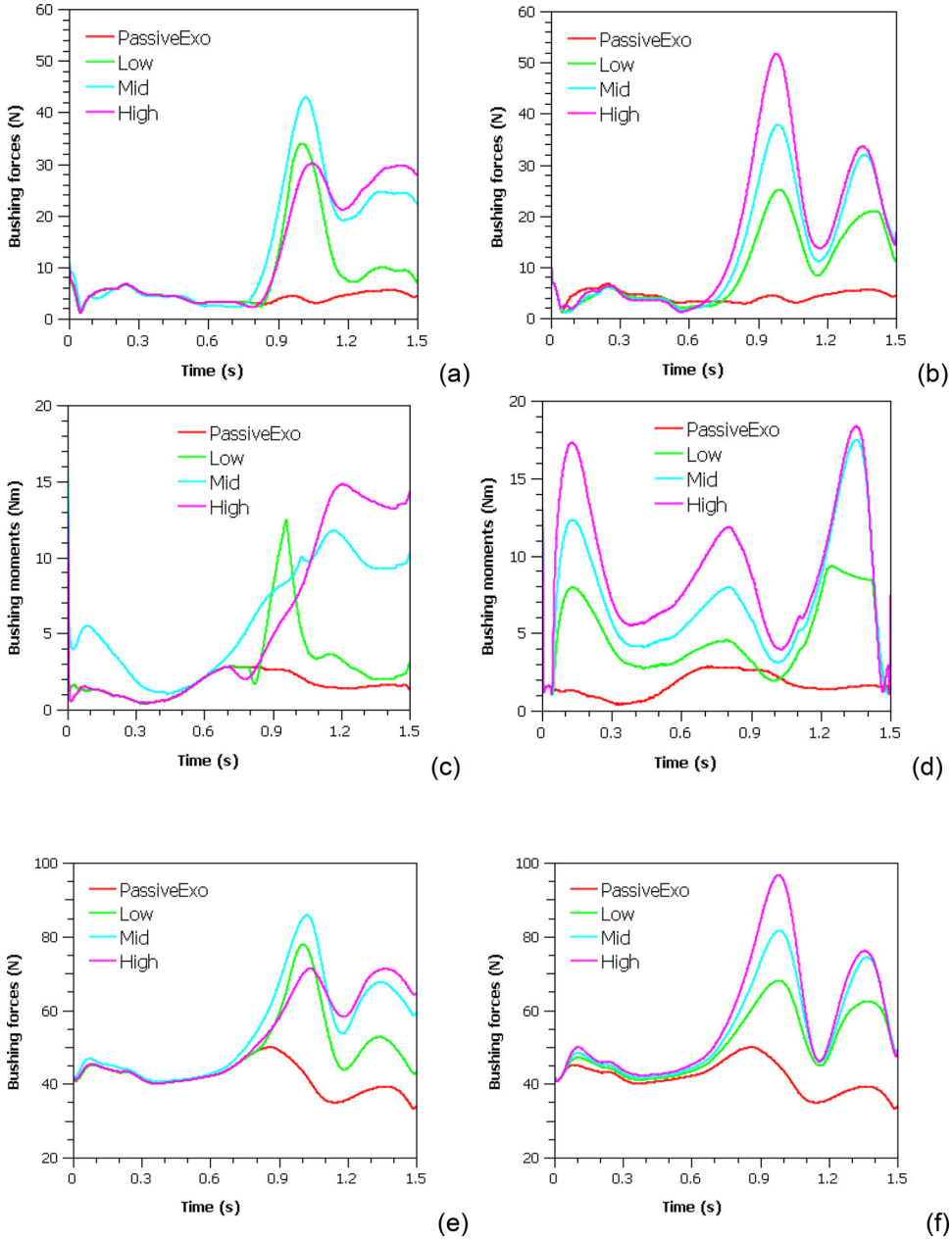

Figure 6. Bushing forces (top row) and moments (middle row) between the exoskeleton armbar and the human upper arm, and bushing forces between the exoskeleton base and the human torso (bottom row). Results are shown separately for the spring-assist passive exoskeleton (left column) and the EMG-based active exoskeleton (right column).

moment reductions (Figure 7) and the shoulder joint velocities, and the results are shown in Figure 8(e and f). Note that the reductions in Figure 7 were presented as negative but here we flipped them to positive. By integrating the positive and negative powers separately, we obtained the positive and negative work done by the exoskeleton with both mechanical and assistance works listed in Table 4. We further computed the positive work efficiency for each case, defined as the ratio between the positive assistance work and the corresponding positive mechanical work, and these results are also listed in Table 4. Notice that the efficiencies are all under 80%, with the largest found in the EMG-High case.

In Figure 9, activations of the anterior and middle deltoid muscles are shown. In the NoExo case, anterior deltoid activation was relatively high, within the range of $0.2 - 0.7$, whereas the middle deltoid had low activation (<0.2) at the first half of the simulation and then started to increase rapidly. At the end of the simulation, activations declined for both muscles due to shoulder stop and deacceleration for weight placement. Considering this, we chose the anterior deltoid instead of the middle deltoid as the source for EMG

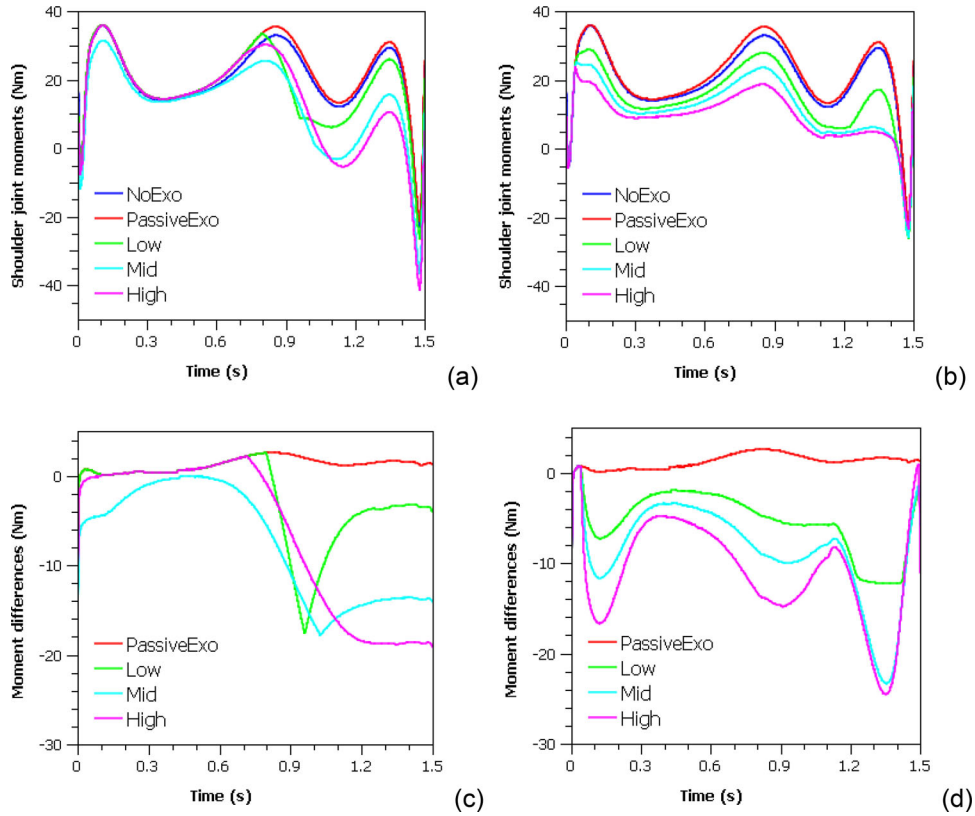

Figure 7. Human shoulder joint moments with and without (a) the spring-assist passive exoskeleton and (b) the EMG-based active exoskeleton. Differences in shoulder joint moments between cases with the exoskeleton and the baseline NoExo case are shown for (c) the spring-assist passive exoskeleton and (d) the EMG-based active exoskeleton.

assistance because it can achieve larger activation reduction with assistance. For the spring-assist cases, reductions in muscle activations were mainly observed during the second half of the lifting motion, when the exoskeleton entered the activation zones. For the EMG-based active cases, the reductions seem to be proportional to the baseline activation during the entire simulation. In Table 5, root-mean-square (RMS) levels of muscle activation are listed for all cases. The Spring-Mid case reduced RMS of the anterior deltoid the most, by 25.9%, and the Spring-High case reduced the RMS of middle deltoid the most, by 54%. Among the EMG-assist cases, the EMG-High case performed the best and reduced the RMS of the anterior and middle deltoid muscles by 51.4 and 61.1%, respectively.

Due to changes in muscle activations and forces, the shoulder joint reaction forces varied accordingly, and Figure 10 compares the magnitudes of total joint reaction forces for all cases. For the NoExo and PassiveExo cases, the maximum joint reaction force was close to 2933*N*. For the spring-assist passive cases, large reductions were observed during 1-1.2 seconds but then the force quickly climbed over 2500*N* for all cases. For the EMG-based active cases, the reductions again seem to be proportional. The lowest maximum force for the spring-assist cases was 2659 N (Spring-High) and for EMG-assist cases was 1580 N (EMG-High).

4. Discussion

In a recent review by McFarland and Fischer (2019), a good amount of evidence supported the efficacy of passive upper limb exoskeletons in reducing muscular activities of the anterior and middle deltoid during occupational tasks, primarily those tasks involving overhead work. However, there are fewer studies to show the efficacy of powered active upper limb exoskeletons. In this study, our simulations indicated the benefits of both passive and active assistances and indicated that EMG-based active assistance may achieve better results for one design that mimics a commercial device template. The choice of the exoskeleton template is likely to impact the findings, since other devices may use different kinematic structures or actuation methods. However, we anticipate similar trends and observations, as long as the design has similar assistance and interference with the wearer's motion.

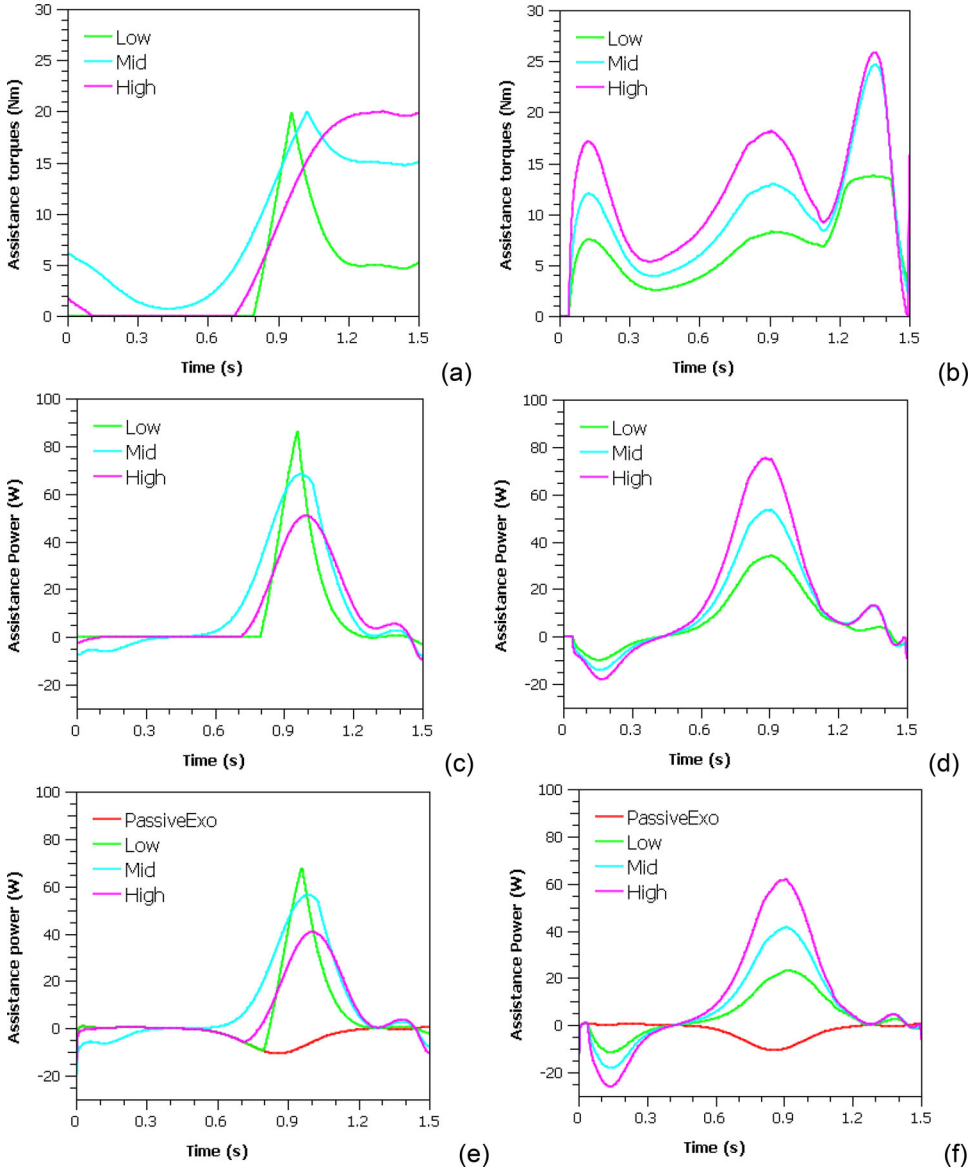

Figure 8. Exoskeleton joint torques (top row) and mechanical powers (middle row) generated by the spring-assist passive exoskeleton (left column) and the EMG-based active exoskeleton (right column). The bottom row is the assistance powers transmitted to the human shoulder joint.

Table 4. Positive and negative work (unit J) done by the exoskeleton under different conditions and the efficiencies of the positive work. Positive and negative works are split by a "/", and the work done by the passive exoskeleton is $+0.17/-3.67J$. "Exo" means the mechanical work while "Human" means the transmitted assistance work.

	Spring-assist			EMG-assist		
Work	Exo	Human	Efficiency	Exo	Human	Efficiency
Low	+13.58/-0.11	+10.55/-1.44	77.7%	+13.07/-2.11	+8.66/-2.23	66.3%
Mid	+21.63/-1.75	+16.48/-1.80	76.2%	+20.44/-3.07	+14.98/-3.47	73.3%
High	+16.12/-0.42	+11.13/-1.24	69.0%	+27.10/-3.80	+21.43/-4.80	79.1%

Our simulation reasonably predicted that the fully passive exoskeleton (PassiveExo) added small extra load to the shoulder joints, since the exoskeleton presented in this study is relatively light (4.3 kg). This result shows that the design of the exoskeleton is compliant to the human's lifting motion. Unsurprisingly, the arm bushing forces and moments in the PassiveExo case were much smaller than those of the assistance cases. Among the spring-assist exoskeleton cases, the Mid case produced the highest

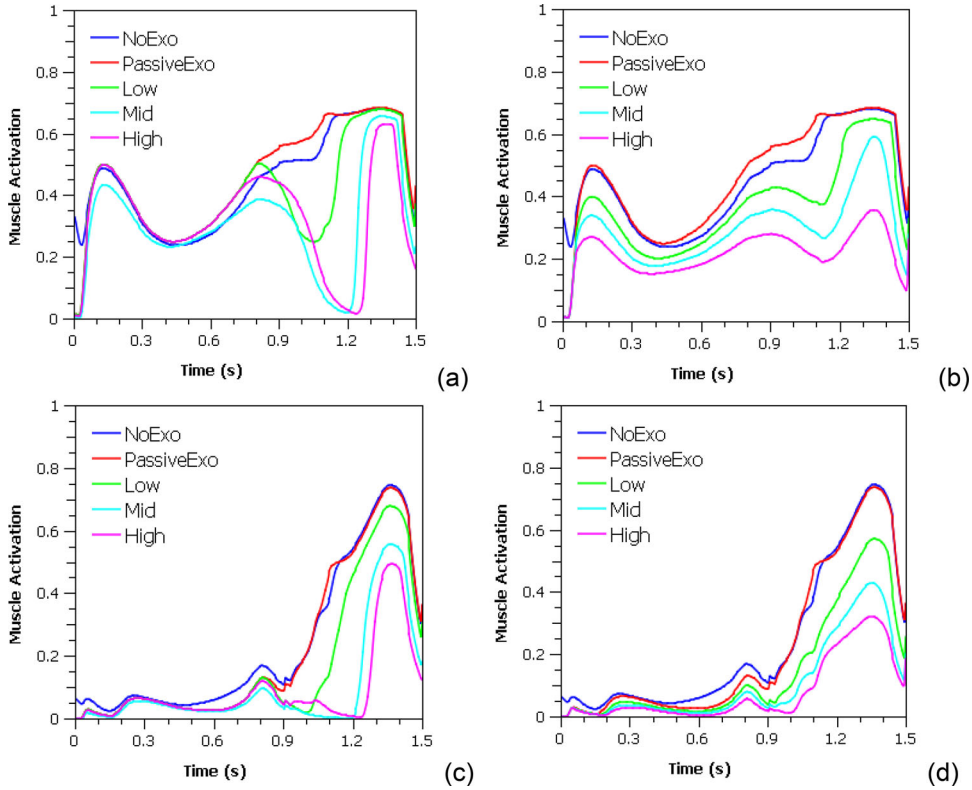

Figure 9. Activations of the anterior deltoid (top row) and the middle deltoid (bottom row) muscles with the spring-assist passive exoskeleton (left column) and the EMG-based active exoskeleton (right column).

Table 5. Comparison of muscle activations (RMS).

			Spring-assist			EMG-assist		
	NoExo	PassiveExo	Low	Mid	High	Low	Mid	High
Anterior Deltoid	0.471	0.493	0.435	0.350	0.361	0.394	0.316	0.229
(% Difference)	–	4.7	−7.8	−25.9	−23.4	−16.4	−32.9	−51.4
Middle Deltoid	0.332	0.329	0.275	0.189	0.152	0.231	0.169	0.129
(% Difference)	–	−0.9	−17.2	−43.1	−54.0	−30.3	−49.1	−61.1

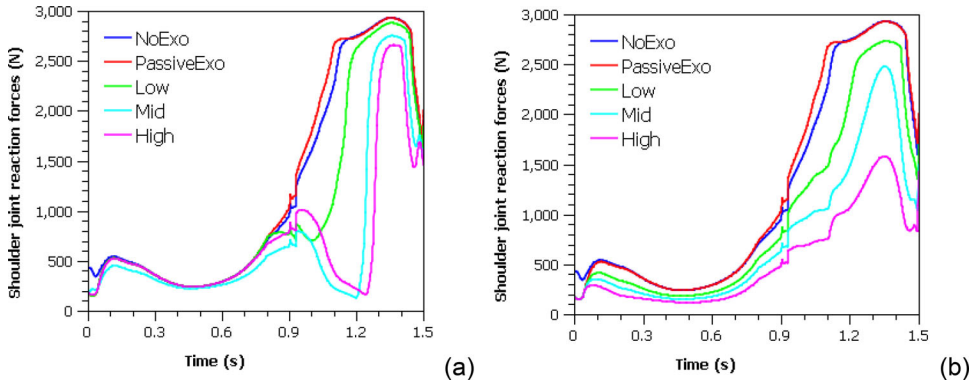

Figure 10. Comparison of the total shoulder joint reaction forces for (a) the spring-assist passive exoskeleton and (b) the EMG-based active exoskeleton.

peak bushing force while the High case produced larger force than the Low and Mid cases when the upper arm was more than 20° above the horizontal plane, at which the Low case generated the smallest bushing force (around or less than 10 N). This clearly indicates that the Low case is less effective in assisting overhead lifting when the elevation is high, whereases the High case is the most effective. For the EMG-assist cases, the bushing forces were in similar patterns with the magnitudes in an increasing order of

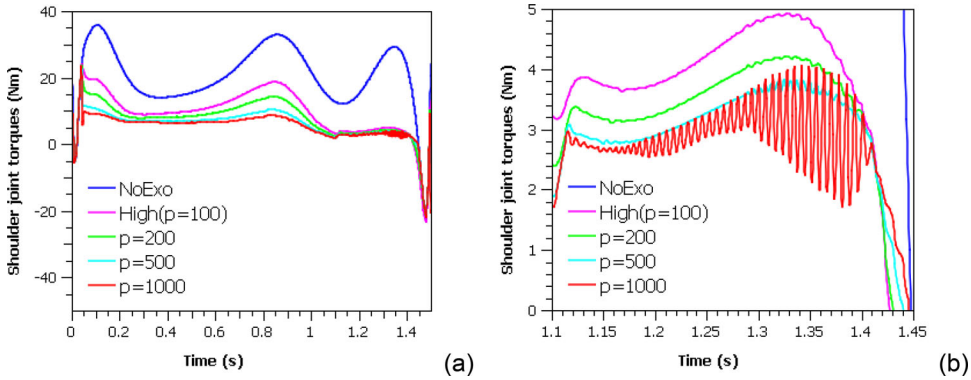

Figure 11. (a) Human shoulder joint moments with high proportional gains for the EMG-based active exoskeleton; (b) Zoom-in view of the moments between 1.1 to 1.45 seconds.

Low, Mid, and High, which shows good consistency in generating assistance during the entire phase of lifting. For the spring assistance cases, reductions in biomechanical loadings happened mainly at a certain range of the lifting motion—specifically the second half of the motion—when the armbar enters the activation zones. The Mid activation zone case did more positive and negative work than the other two cases and performed much better than the Low activation case and comparably to the High activation case in reducing muscle activations and joint reaction forces. On the other hand, the EMG-based active assistance contributed to a reduction of biomechanical loadings during the entire course of the motion, and the reduction was proportional to the muscle EMG in nature. Even when the assistance performed relatively large negative power during the initial arm retraction phase (due to large positive torque but negative velocity), activation of the anterior deltoid muscle was reduced because the positive torques helped to resist the lifting weight during arm retraction. The muscle activation and produced assistance torque mutually affected each other during the simulation. In general, higher EMG gain produces better performance. As it is evident from Figure 11, however, the gain should be limited to avoid reaching instability. One potential future work is to test variable gains that depend on the instantaneous EMG level and investigate the stability and benefits of such gains.

Compared to the spring-assist cases, the best EMG-assist case (EMG-High) achieved much higher reductions in both muscle activations and shoulder joint reaction force. The EMG-High case reduced the joint reaction force by 46.1% compared to the NoExo case, whereas the best spring-assist (Spring-High) case only reduced the force by 9.3%. Despite the potential benefits of using EMG-based active assistance in exoskeletons, there are multiple challenges in this assistance approach. First, the EMG-assist device with added components such as motors, battery, and cables, is heavier and requires the use of a surface EMG sensor on the skin that could be inconvenient when the user wears occupational clothing. Second, the raw surface EMG signal in practice is often noisy and needs real-time pre-processing before entering the controller. In general, EMG can be processed by high and low pass filtering, rectification, and normalization with respect to the maximal level to generate a suitable input signal (Li et al., 2017). In several studies, RMS of EMG was used for controller input (Kiguchi & Hayashi, 2012; Rahman et al., 2015; Tang et al., 2014). In this study, only one muscle, the anterior deltoid, was used for EMG based control, which could trigger unintentional actuation. For example, the exoskeleton could be actuated when the anterior deltoid is activated as an antagonist muscle (Assila et al., 2020; Blache et al., 2015) or when the shoulder decelerates to release the weight. The use of an EMG threshold (10% MVC in Eq. (2)) can help filter out unintentional triggers such as EMG noises or small co-contraction signal but may not be good enough in some cases. Therefore, it might be beneficial to consider the torque assistance with input from multiple agonistic and antagonistic muscles.

Due to the lack of experiment data, our model and simulation were compared with data from several previous studies. For the no exoskeleton case, we compared the deltoid muscle activations to data available in the literature for overhead lifting (Assila et al., 2020; Blache et al., 2015) and observed similar trends of activation and timing despite differences in lifting weights and heights. The pattern of the joint reaction forces are similar to that reported *in vivo* using an instrumented prosthesis (Bergmann et al., 2007; Westerhoff et al., 2009) and via modeling (Assila et al., 2020; Martinez et al., 2020). The amplitudes are much higher than the *in vivo* measurements

($\sim 1000\boldsymbol{N}$) but close to the modeling results ($\sim$3000 N). Note that in the *in vivo* study (Bergmann et al., 2007) the lifting mass is only 2 kg and the lifting velocity was quite slower ($\sim$4 s for shoulder elevation). Also, in the modeling study (Assila et al., 2020; Martinez et al., 2020) the lifting height was to the eye level. These differences in lifting weight and kinematics are likely the major factors for the difference in joint reaction forces. Another possible contributing factor could be the accuracy of muscle moment arms for overhead postures. Small muscle moment arms tend to artificially increase the joint reaction force.

5. Conclusions

In this work, we conducted model-based human-exoskeleton interaction simulations to compare passive and active assistance designs of an occupational upper limb exoskeleton for overhead lifting. An upper extremity musculoskeletal model was integrated with an exoskeleton for virtual human-in-the-loop evaluation of exoskeleton design and control. Different assistance methods were evaluated to study their biomechanical effects on the wearer' musculoskeletal loadings. By comparing the biomechanical loadings, we showed the efficacy of both spring-based passive assistance and EMG-based active assistance methods. In addition, our simulation results indicated that the EMG-based active assistance approach could achieve greater reductions in shoulder joint reaction forces and provide assistance over a larger lifting range. In the future, we plan to conduct parametric simulations and human-subject experiments to further optimize the exoskeleton assistance methods and prove their effectiveness for different subjects and overhead lifting conditions with different speeds, heights, and directions.

Acknowledgments

N/A

Conflict of Interest

The authors declare no conflict of interest.

Funding

This research was supported by a startup grant to Dr. Zhou from New Jersey Institute of Technology. The contents of this paper are solely the responsibility of the authors and do not necessarily represent the official position of New Jersey Institute of Technology and the National Institute for Occupational Safety and Health, Centers for Disease Control and Prevention.

ORCID

Xianlian Zhou http://orcid.org/0000-0001-9282-5410

References

Alabdulkarim, S., & Nussbaum, M. A. (2019). Influences of different exoskeleton designs and tool mass on physical demands and performance in a simulated overhead drilling task. *Applied Ergonomics*, *74*, 55–66. https://doi.org/10.1016/j.apergo.2018.08.004

Assila, N., Pizzolato, C., Martinez, R., Lloyd, D. G., & Begon, M. (2020). EMG-assisted algorithm to account for shoulder muscles co-contraction in overhead manual handling. *Applied Sciences*, *10*(10), 3522. https://doi.org/10.3390/app10103522

Bergmann, G., Graichen, F., Bender, A., Kääb, M., Rohlmann, A., & Westerhoff, P. (2007). In vivo glenohumeral contact forces-measurements in the first patient 7 months postoperatively. *Journal of Biomechanics*, *40*(10), 2139–2149. https://doi.org/10.1016/j.jbiomech.2006.10.037

Bernard, B. P., & Putz-Anderson, V. (1997). Musculoskeletal disorders and workplace factors; A critical review of epidemiologic evidence for work-related musculoskeletal disorders of the neck, upper extremity, and low back. In: Bernard, B. P. (ed.), National Institute for Occupational Safety and Health, U. S. Department of Health and Human Services, Publication No. 97B141, Cincinnati, OH.

Blache, Y., Dal Maso, F., Desmoulins, L., Plamondon, A., & Begon, M. (2015). Superficial shoulder muscle co-activations during lifting tasks: Influence of lifting height, weight and phase. *Journal of Electromyography and Kinesiology*, *25*(2), 355–362. https://doi.org/10.1016/j.jelekin.2014.11.004

Blache, Y., Desmoulins, L., Allard, P., Plamondon, A., & Begon, M. (2015). Effects of height and load weight on shoulder muscle work during overhead lifting task. *Ergonomics*, *58*(5), 748–761. https://doi.org/10.1080/00140139.2014.980336

Bogue, R. (2018). Exoskeletons–a review of industrial applications. *Industrial Robot: An International Journal*, *45*(5), 585–590. https://doi.org/10.1108/IR-05-2018-0109

Bureau of Labor Statistics, & U.S. Department of Labor. (2018). Back injuries prominent in work-related musculoskeletal disorder cases in 2016. *The Economics Daily, on the Internet at* https://www.bls.gov/opub/ted/2018/back-injuries-prominent-in-work-related-musculoskeletal-disorder-cases-in-2016.htm.

Chopp, J. N., Fischer, S. L., & Dickerson, C. R. (2010). The impact of work configuration, target angle and hand force direction on upper extremity muscle activity during sub-maximal overhead work. *Ergonomics*, *53*(1), 83–91. https://doi.org/10.1080/00140130903323232

Constantinescu, C., Muresan, P.-C., & Simon, G.-M. (2016). JackEx: The new digital manufacturing resource for optimization of exoskeleton-based factory environments. *Procedia CIRP*, *50*, 508–511. https://doi.org/10.1016/j.procir.2016.05.048

Constantinescu, C., Todorovic, O., & Ippolito, D. (2019). Comprehensive modelling and simulation towards the identification of critical parameters for evaluation of

exoskeleton-centred workplaces. *Procedia CIRP*, *79*, 176–179. https://doi.org/10.1016/j.procir.2019.02.040

Damsgaard, M., Rasmussen, J., Christensen, S. T., Surma, E., & de Zee, M. (2006). Analysis of musculoskeletal systems in the AnyBody Modeling System. *Simulation Modelling Practice and Theory*, *14*(8), 1100–1111. https://doi.org/10.1016/j.simpat.2006.09.001

de Looze, M. P., Bosch, T., Krause, F., Stadler, K. S., & O'Sullivan, L. W. (2016). Exoskeletons for industrial application and their potential effects on physical work load. *Ergonomics*, *59*(5), 671–681. https://doi.org/10.1080/00140139.2015.1081988

Del Ferraro, S., Falcone, T., Ranavolo, A., & Molinaro, V. (2020). The effects of upper-body exoskeletons on human metabolic cost and thermal response during work tasks—A systematic review. *International Journal of Environmental Research and Public Health*, *17*(20), 7374. https://doi.org/10.3390/ijerph17207374

Delp, S. L., Anderson, F. C., Arnold, A. S., Loan, P., Habib, A., John, C. T., Guendelman, E., & Thelen, D. G. (2007). OpenSim: Open-source software to create and analyze dynamic simulations of movement. *IEEE Transactions on Bio-Medical Engineering*, *54*(11), 1940–1950. https://doi.org/10.1109/TBME.2007.901024

Dembia, C. L., Silder, A., Uchida, T. K., Hicks, J. L., & Delp, S. L. (2017). Simulating ideal assistive devices to reduce the metabolic cost of walking with heavy loads. *PLoS One*, *12*(7), e0180320. https://doi.org/10.1371/journal.pone.0180320

Erdemir, A., McLean, S., Herzog, W., & van den Bogert, A. J. (2007). Model-based estimation of muscle forces exerted during movements. *Clinical Biomechanics (Bristol, Avon)*, *22*(2), 131–154. https://doi.org/10.1016/j.clinbiomech.2006.09.005

Fougner, A., Stavdahl, Ø., Kyberd, P. J., Losier, Y. G., & Parker, P. A. (2012). Control of upper limb prostheses: Terminology and proportional myoelectric control-a review. *IEEE Transactions on Neural Systems and Rehabilitation Engineering : A Publication of the IEEE Engineering in Medicine and Biology Society*, *20*(5), 663–677. https://doi.org/10.1109/TNSRE.2012.2196711

Gopura, R., Bandara, D., Kiguchi, K., & Mann, G. K. (2016). Developments in hardware systems of active upper-limb exoskeleton robots: A review. *Robotics and Autonomous Systems*, *75*, 203–220. https://doi.org/10.1016/j.robot.2015.10.001

Gopura, R., Kiguchi, K., & Bandara, D. (2011). *A brief review on upper extremity robotic exoskeleton systems* [Paper presentation]. 2011 6th International Conference on Industrial and Information Systems.

Grieve, J. R., & Dickerson, C. R. (2008). Overhead work: Identification of evidence-based exposure guidelines. *Occupational Ergonomics*, *8*(1), 53–66. https://doi.org/10.3233/OER-2008-8105

Islam, M. R., Spiewak, C., Rahman, M. H., & Fareh, R. (2017). A brief review on robotic exoskeletons for upper extremity rehabilitation to find the gap between research porotype and commercial type. *Advances in Robotics & Automation*, *06*(03), 2. https://doi.org/10.4172/2168-9695.1000177

Kiguchi, K., & Hayashi, Y. (2012). An EMG-based control for an upper-limb power-assist exoskeleton robot. *IEEE Transactions on Systems, Man, and Cybernetics, Part B (Cybernetics)*, *42*(4), 1064–1071. https://doi.org/10.1109/TSMCB.2012.2185843

Kim, S., Nussbaum, M. A., Esfahani, M. I. M., Alemi, M. M., Alabdulkarim, S., & Rashedi, E. (2018a). Assessing the influence of a passive, upper extremity exoskeletal vest for tasks requiring arm elevation: Part I – "Expected" effects on discomfort, shoulder muscle activity, and work task performance. *Applied Ergonomics*, *70*, 315–322. https://doi.org/10.1016/j.apergo.2018.02.025

Kim, S., Nussbaum, M. A., Esfahani, M. I. M., Alemi, M. M., Jia, B., & Rashedi, E. (2018b). Assessing the influence of a passive, upper extremity exoskeletal vest for tasks requiring arm elevation: Part II - "Unexpected" effects on shoulder motion, balance, and spine loading. *Applied Ergonomics*, *70*, 323–330. https://doi.org/10.1016/j.apergo.2018.02.024

Li, Z., Huang, Z., He, W., & Su, C.-Y. (2017). Adaptive impedance control for an upper limb robotic exoskeleton using biological signals. *IEEE Transactions on Industrial Electronics*, *64*(2), 1664–1674. https://doi.org/10.1109/TIE.2016.2538741

Li, Z., Wang, B., Sun, F., Yang, C., Xie, Q., & Zhang, W. (2014). sEMG-based joint force control for an upper-limb power-assist exoskeleton robot. *IEEE Journal of Biomedical and Health Informatics*, *18*(3), 1043–1050. https://doi.org/10.1109/JBHI.2013.2286455

Lo, H. S., & Xie, S. Q. (2012). Exoskeleton robots for upper-limb rehabilitation: State of the art and future prospects. *Medical Engineering & Physics*, *34*(3), 261–268. https://doi.org/10.1016/j.medengphy.2011.10.004

Martinez, R., Assila, N., Goubault, E., & Begon, M. (2020). Sex differences in upper limb musculoskeletal biomechanics during a lifting task. *Applied Ergonomics*, *86*, 103106. https://doi.org/10.1016/j.apergo.2020.103106

Maurice, P., Camernik, J., Gorjan, D., Schirrmeister, B., Bornmann, J., Tagliapietra, L., Latella, C., Pucci, D., Fritzsche, L., Ivaldi, S., & Babic, J. (2020). Objective and subjective effects of a passive exoskeleton on overhead work. *IEEE Transactions on Neural Systems and Rehabilitation Engineering : A Publication of the IEEE Engineering in Medicine and Biology Society*, *28*(1), 152–164. https://doi.org/10.1109/TNSRE.2019.2945368

McFarland, T., & Fischer, S. (2019). Considerations for industrial use: A systematic review of the impact of active and passive upper limb exoskeletons on physical exposures. *IISE Transactions on Occupational Ergonomics and Human Factors*, *7*(3–4), 322–347. https://doi.org/10.1080/24725838.2019.1684399

Miranda, H., Viikari-Juntura, E., Heistaro, S., Heliövaara, M., & Riihimäki, H. (2005). A population study on differences in the determinants of a specific shoulder disorder versus nonspecific shoulder pain without clinical findings. *American Journal of Epidemiology*, *161*(9), 847–855. https://doi.org/10.1093/aje/kwi112

Mirtich, B. (1996). Fast and accurate computation of polyhedral mass properties. *Journal of Graphics Tools*, *1*(2), 31–50. https://doi.org/10.1080/10867651.1996.10487458

Mokrani, M. W. (2009). *Neck muscles activity and upper body extremity angles in dynamic overhead lifting* [Master thesis]. Louisiana State University and Agricultural and Mechanical College.

Nussbaum, M. A., Lowe, B. D., de Looze, M., Harris-Adamson, C., & Smets, M. (2019). *An introduction to the special issue on occupational exoskeletons*. Taylor & Francis.

Punnett, L., Fine, L. J., Keyserling, W. M., Herrin, G. D., & Chaffin, D. B. (2000). Shoulder disorders and postural stress in automobile assembly work. *Scandinavian Journal of Work, Environment & Health*, *26*(4), 283–291. https://doi.org/10.5271/sjweh.544

Rahman, M. H., Ochoa-Luna, C., Saad, M., & Archambault, P. (2015). EMG based control of a robotic exoskeleton for shoulder and elbow motion assist. *Journal of Automation and Control Engineering*, *3*(4), 270–276.

Saul, K. R., Hu, X., Goehler, C. M., Vidt, M. E., Daly, M., Velisar, A., & Murray, W. M. (2015). Benchmarking of dynamic simulation predictions in two software platforms using an upper limb musculoskeletal model. *Computer Methods in Biomechanics and Biomedical Engineering*, *18*(13), 1445–1458. https://doi.org/10.1080/10255842.2014.916698

Schmalz, T., Schändlinger, J., Schuler, M., Bornmann, J., Schirrmeister, B., Kannenberg, A., & Ernst, M. (2019). Biomechanical and metabolic effectiveness of an industrial exoskeleton for overhead work. *International Journal of Environmental Research and Public Health*, *16*(23), 4792. https://doi.org/10.3390/ijerph16234792

Schutte, L. M., Rodgers, M. M., Zajac, F. E., & Glaser, R. M. (1993). Improving the efficacy of electrical stimulation-induced leg cycle ergometry: An analysis based on a dynamic musculoskeletal model. *IEEE Transactions on Rehabilitation Engineering*, *1*(2), 109–125. https://doi.org/10.1109/86.242425

Serrancolí, G., Falisse, A., Dembia, C., Vantilt, J., Tanghe, K., Lefeber, D., Jonkers, I., De Schutter, J., & De Groote, F. (2019). Subject-exoskeleton contact model calibration leads to accurate interaction force predictions. *IEEE Transactions on Neural Systems and Rehabilitation Engineering*, *27*(8), 1597–1605. https://doi.org/10.1109/TNSRE.2019.2924536

Tang, Z., Zhang, K., Sun, S., Gao, Z., Zhang, L., & Yang, Z. (2014). An upper-limb power-assist exoskeleton using proportional myoelectric control. *Sensors*, *14*(4), 6677–6694. https://doi.org/10.3390/s140406677

Uchida, T. K., Seth, A., Pouya, S., Dembia, C. L., Hicks, J. L., & Delp, S. L. (2016). Simulating ideal assistive devices to reduce the metabolic cost of running. *PLoS One*, *11*(9), e0163417. https://doi.org/10.1371/journal.pone.0163417

Westerhoff, P., Graichen, F., Bender, A., Halder, A., Beier, A., Rohlmann, A., & Bergmann, G. (2009). In vivo measurement of shoulder joint loads during activities of daily living. *Journal of Biomechanics*, *42*(12), 1840–1849. https://doi.org/10.1016/j.jbiomech.2009.05.035

Zhou, L., Bai, S., Andersen, M. S., & Rasmussen, J. (2015). Modeling and design of a spring-loaded, cable-driven, wearable exoskeleton for the upper extremity. *Modeling, Identification and Control: A Norwegian Research Bulletin*, *36*(3), 167–177. https://doi.org/10.4173/mic.2015.3.4

Zhou, X., & Chen, X. (2021). Design and evaluation of torque compensation controllers for a lower extremity exoskeleton. *Journal of Biomechanical Engineering*, *143*(1), 11. https://doi.org/10.1115/1.4048572

Zhou, X., Whitley, P., & Przekwas, A. (2014). A musculoskeletal fatigue model for prediction of aviator neck maneuvering loadings. *International Journal of Human Factors Modelling and Simulation*, *4*(3/4), 191–219. https://doi.org/10.1504/IJHFMS.2014.067174

Zhu, Z., Dutta, A., & Dai, F. (2021). Exoskeletons for manual material handling–A review and implication for construction applications. *Automation in Construction*, *122*, 103493. https://doi.org/10.1016/j.autcon.2020.103493

Appendix

A1. The Effects of EMG-Assist Gain Parameter (p)

To evaluate the sensitivity of the EMG-based control to the gain parameter p and find potential optimal p, we numerically experimented with higher gains at $p = 200$, 500, and 1000. In Figure 11, the shoulder joint moments are compared for all these high gain cases with the NoExo case and the EMG-High case ($p = 100$) added as references. As it can be seen, using higher gains further reduced the joint moment at the early phase of the lifting. When the lifting was above the shoulder, the moments were reduced from over 30Nm to less than 5Nm for all active cases and obvious oscillation can be observed with the worst case being the one with the highest gain ($p = 1000$). It is possible the oscillation may be a simulation artifact and the oscillatory gain values are likely depending on the simulation set up such as the bushing parameters. In reality, the oscillation may be avoided or minimized if the hardware is tuned or straps are adjusted properly. Therefore, the importance of setting up proper bushing parameters in simulations shall not be overlooked (Serrancolí et al., 2019).

A2. Spring Assistance with the High Activation Zone at Different Assistance Levels

We conducted simulations of spring assistance with the High activation zone at three different assistance level (15, 20, and 25Nm) to compare their loadings on the musculoskeletal system. Detailed results for the 20Nm assistance are presented in the main text. The 25Nm torque assistance is very close to the maximum EMG-based assistance torque. Figure 12 shows the bushing forces and moments between the exoskeleton and the human. As expected, increasing the level of assistance increased the bushing forces and moments. Figure 13 shows the activations of the anterior and middle deltoid muscles and Figure 14 compares the shoulder joint reaction forces. Evidently, increasing the level of assistance decreased both the muscle activations and joint reaction forces. For the assistance torque of 25Nm, we found the maximum joint reduction force to be 2439N, which is the smallest among all spring assistances.

A3. Parametric Study with Doubled Bushing Parameters

To investigate the effects of bushing parameters, we doubled all the bushing parameters in Table 2 and those for the bushing at the base and ran several simulations including

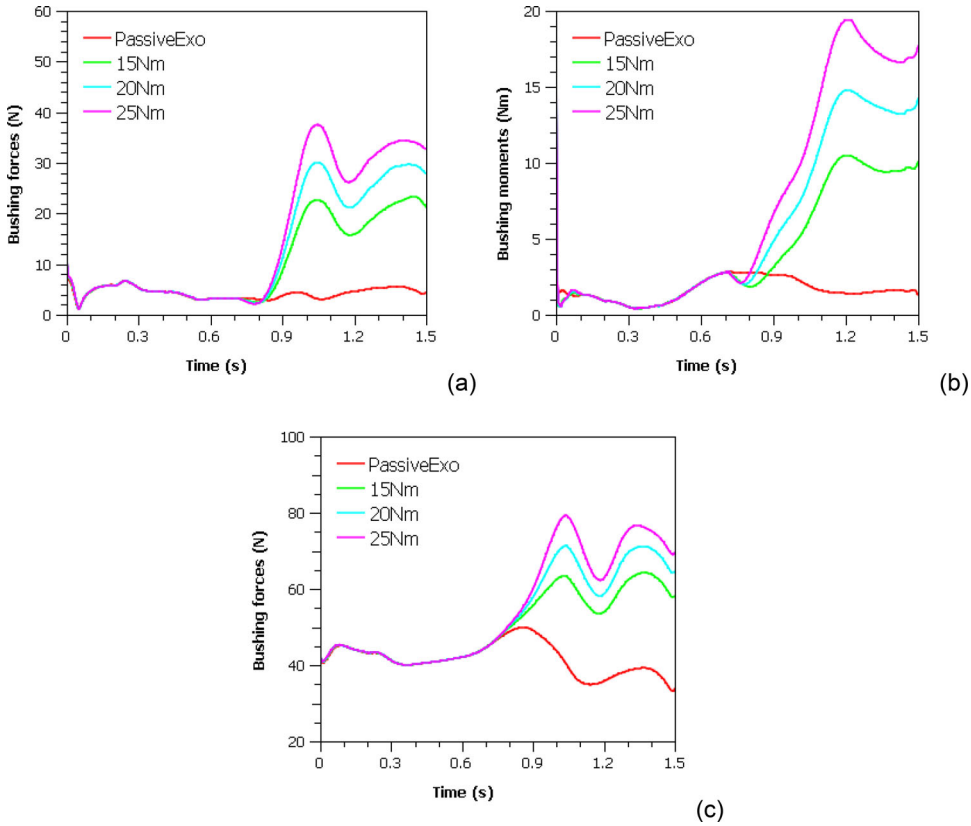

Figure 12. (a) Bushing forces and (b) moments between the exoskeleton armbar and the human arm and (c) bushing forces between the exoskeleton base and the human torso for the spring-assist exoskeleton with the High activation zone at three different assistance levels (15Nm, 20Nm, and 25Nm). The PassiveExo (no assistance) case is also included here for comparison.

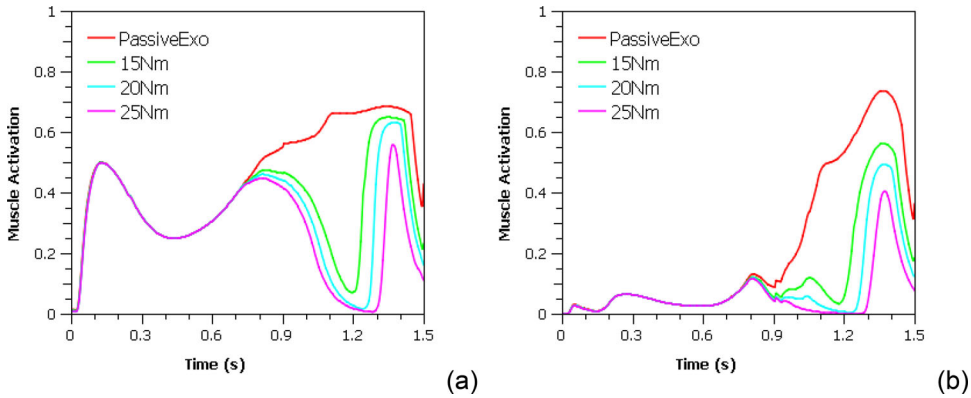

Figure 13. Activations of (a) the anterior deltoid and (b) the middle deltoid muscles for the spring-assist exoskeleton with the High activation zone at three different assistance levels (15Nm, 20Nm, and 25Nm).

the PassiveExo case (PassiveExo-Double), the spring-assist case with the High assistance zone and 25*Nm* maximum torque (Spring-High-25Nm-Double), and the EMG-assist case with the high gain ($p = 100$) (EMG-High-Double). The bushing forces and moments between the exoskeleton and the human are shown in Figure 15. For the PassiveExo cases, doubling the bushing parameters increased both bushing forces and moments at the upper arm by more than 100% and increased the bushing force at the base to a lesser degree. For the Spring-High-25Nm cases, the bushing forces at the arm and base both increased but the bushing moment at the arm decreased by a small amount during the activation zone. Similar trend can be observed for the EMG-High cases. Figure 16 shows the activations of the anterior and middle deltoid muscles and Figure 17 compares the shoulder joint reaction forces. Interestingly, doubling the bushing parameters did not change the muscle activations and shoulder joint reaction forces by much except at around 1.1 seconds with a small spike for the PassiveExo-Double case.

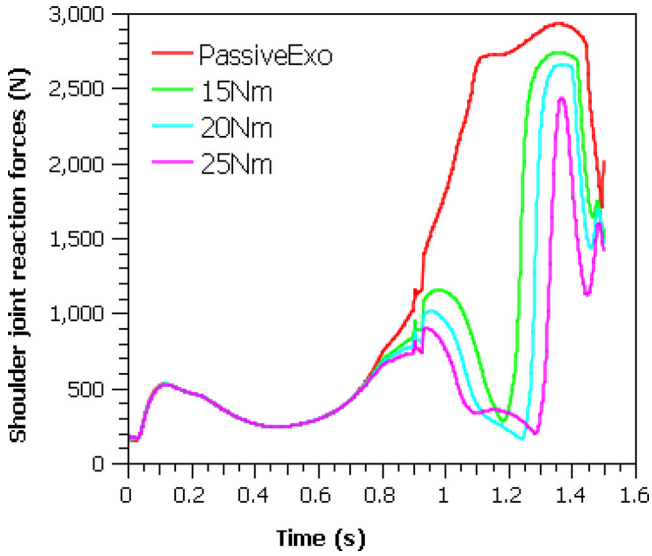

Figure 14. Shoulder joint reaction forces for the spring-assist exoskeleton with the High activation zone at three different assistance levels (15Nm, 20Nm, and 25Nm).

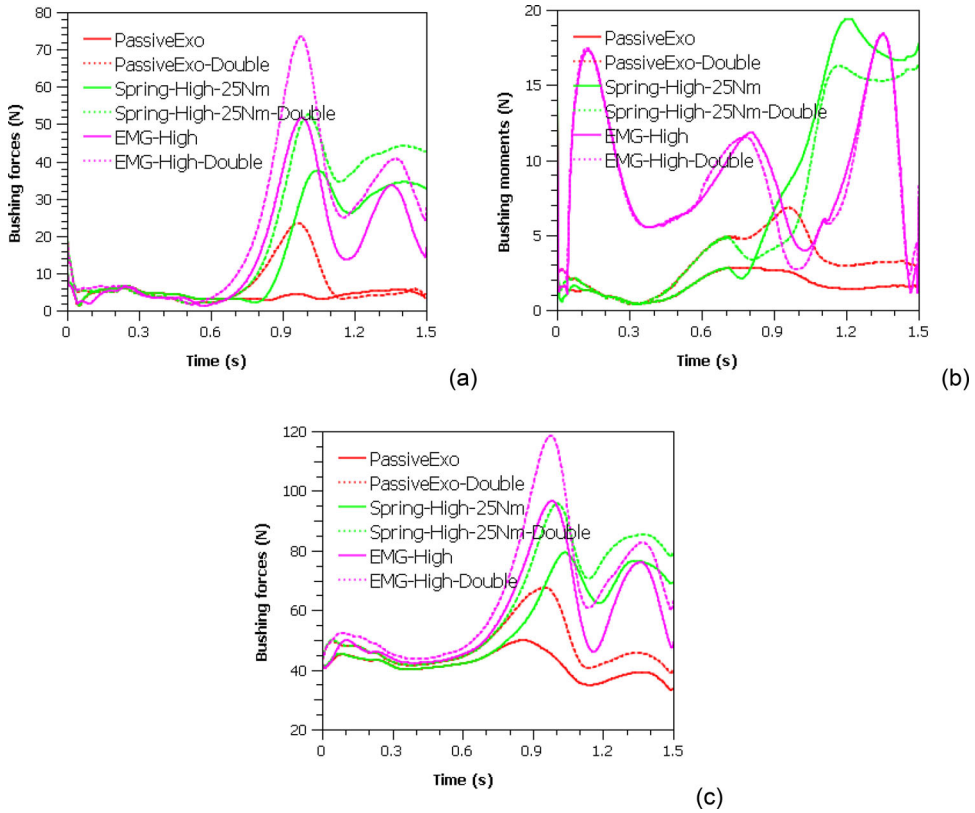

Figure 15. (a) Bushing forces and (b) moments between the exoskeleton armbar and the human upper arm and (c) bushing forces between the exoskeleton base and the human torso with doubled bushing parameters for selected cases.

A4. Parametric Study with Doubled Mass and Inertia Properties

Considering the fact that an active assistance exoskeleton typically contains actuation components such as motors, gears, electronics, and cables that add weight to the passive structure, we investigated the effects of mass properties of the exoskeleton on the loadings to the musculoskeletal system. We doubled the mass and inertia properties of the exoskeleton in Table 1 and conducted additional simulations for the PassiveExo case (PassiveExo-Double) and the EMG-assist case with the High gain ($p = 100$) (EMG-High-Double). Bushing forces and moments between the exoskeleton and the human are shown in Figure 18. For the PassiveExo cases, doubling the mass properties increased all bushing forces and moments with the largest increase seen

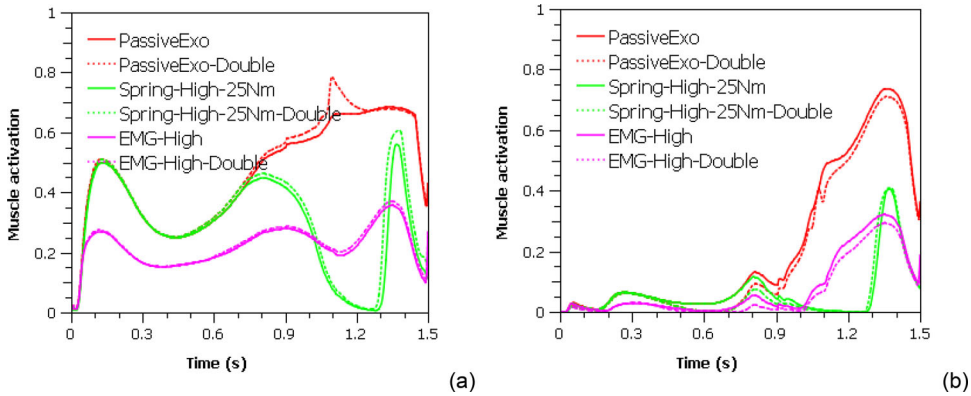

Figure 16. Activations of (a) the anterior deltoid and (b) the middle deltoid muscles with doubled bushing parameters for selected cases.

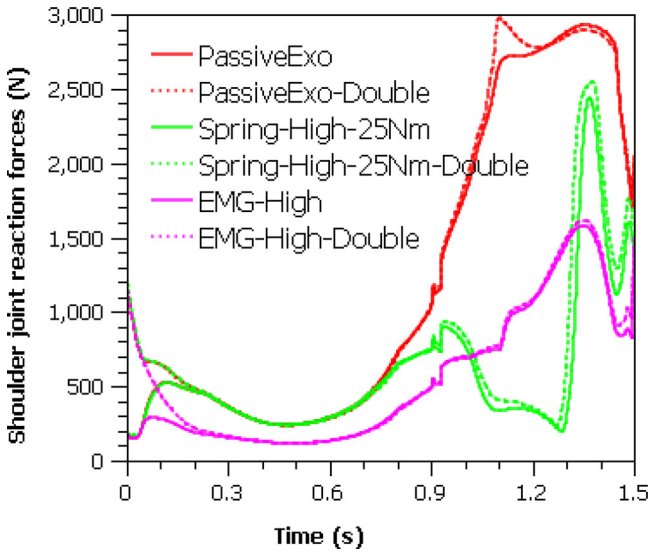

Figure 17. Shoulder joint reaction forces with doubled bushing parameters for selected cases.

for the bushing force at the base (from 49.9*N* to 87.5*N*). For the EMG-High cases, doubling the mass properties increased the bushing force at the base the most (from 96.6*N* to 120.3*N*) but reduced the bushing force at the arm by a smaller amount (from 51.6*N* to 41.5*N*). And the bushing moments for the two EMG-High cases were close to each other. Figure 19 shows the activations of the anterior and middle deltoid muscles and Figure 20 compares the shoulder joint reaction forces. Due to relatively small increase of the total exoskeleton mass by 4.30 kg (including a 1.0 kg increase for the armbar), doubling the mass properties only changed the muscle activations and shoulder joint reaction forces by a small amount during the entire lifting motion.

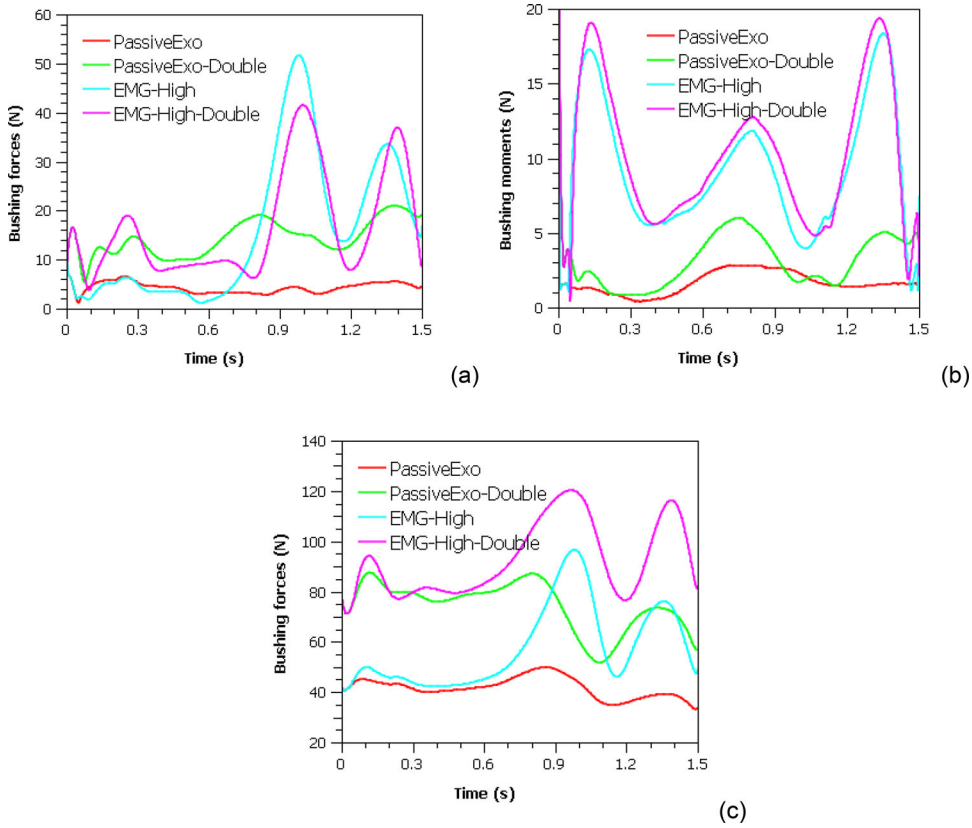

Figure 18. (a) Bushing forces and (b) moments between the exoskeleton armbar and the human upper arm and (c) bushing forces between the exoskeleton base and the human torso with doubled mass properties for selected cases.

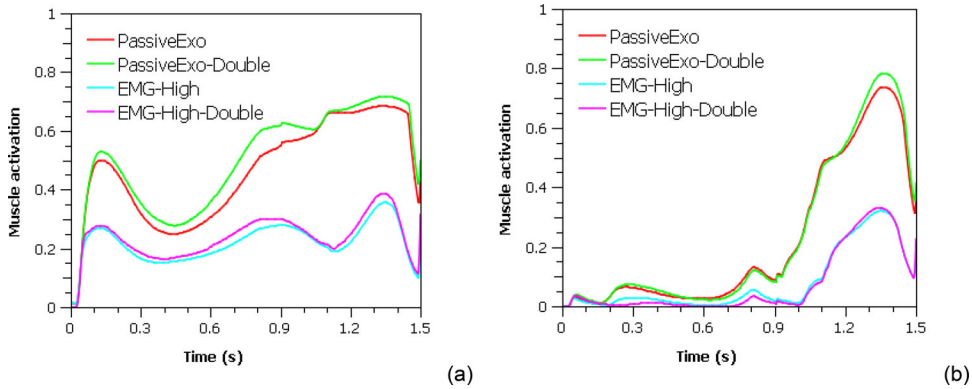

Figure 19. Activations of (a) the anterior deltoid and (b) the middle deltoid muscles with doubled mass properties for selected cases.

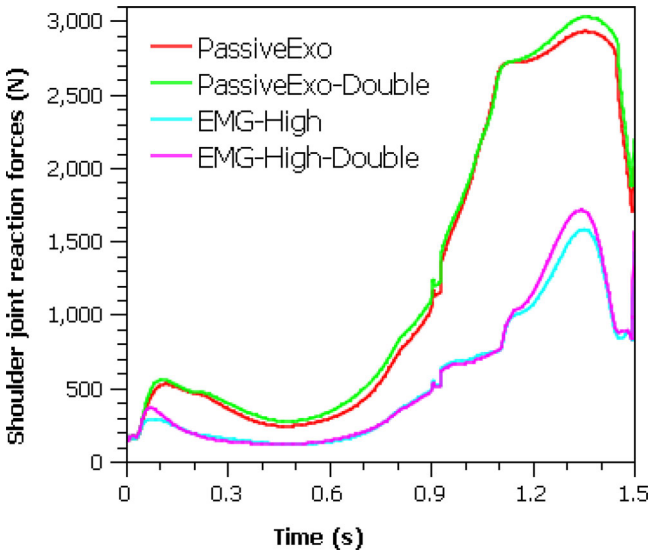

Figure 20. Shoulder joint reaction forces with doubled mass properties for selected cases.